International Journal of Solids and Structures 47 (2010) 427–439

Contents lists available at ScienceDirect

International Journal of Solids and Structures

journal homepage: www.elsevier.com/locate/ijsolstr

Self-piercing riveting connections using aluminium rivets

N.-H. Hoang [a,b,*], R. Porcaro [a,c], M. Langseth [a,b], A.-G. Hanssen [a,b,d]

[a] Structural Impact Laboratory (SIMLab), Centre for Research-based Innovation, Norwegian University of Science and Technology, N-7491 Trondheim, Norway
[b] Department of Structural Engineering, Norwegian University of Science and Technology, N-7491 Trondheim, Norway
[c] SINTEF Materials and Chemistry, N-7465 Trondheim, Norway
[d] Impetus Afea AS, 4400 Flekkefjord, Norway

ARTICLE INFO

Article history:
Received 7 May 2009
Received in revised form 26 August 2009
Available online 13 October 2009

Keywords:
Self-piercing riveting
Aluminium rivet
Aluminium SPR joint
Numerical modelling
Testing

ABSTRACT

The development of the self-piercing riveting (SPR) technology in recent years has broadened the application of the technology in the automobile industry. However, the SPR process currently utilises high-strength steel rivets; and the combination between steel rivets with an aluminium car body makes recycling a challenge. The possibility of replacing a steel self-piercing rivet with an aluminium one has thus been raised as an interesting topic. Within this framework, the objective of the present paper is to provide an experimental database on the riveting process using an aluminium self-piercing rivet. An experimental programme has been carried out, where two similar sheets in aluminium alloy 6060 in three different tempers (temper W, temper T4, and temper T6) have been joined by using a self-piercing rivet in three different alloys, i.e. 6082-T6, 7108-T5, and 7278-T6. The influence of the die shape on the SPR of aluminium sheets using aluminium rivets was also considered. Conventional rivets and dies according to the Boellhoff standards were employed. The test results were exploited in terms of the riveting force–displacement curves and cross-sectional geometries of the riveted joints. The test data were also used to validate a 2D-axisymmetric model, which was originally developed at SIMLab for modelling the riveting process using a steel rivet. Finally, the mechanical behaviour of a riveted connection using an aluminium rivet under quasi-static loading conditions (i.e. combined pure shear and pure opening loads) was experimentally studied and compared with corresponding tests using a steel rivet in terms of force–displacement curves.

1. Introduction

Although the self-piercing riveting (SPR) process is a young joining technology, it has become more and more popular during the last decades, especially in the automotive industry. This is a quick, cheap and single-step technique, using a semi-tubular rivet to fix the sheet components into a mechanical joint. No pre-drilled hole is needed; the rivets are pushed directly into the sheets clamped together between a blank holder and a die in a press tool. The punch, under the pressure conveyed by a hydraulic power device, pushes the rivet to penetrate into the top plate, and the die shape causes the rivet to flare within the lower sheet in order to form a mechanical interlock. The mechanical behaviour of SPR joints strongly depends on the mechanical interlock created within the base materials. The SPR process is illustrated in Fig. 1. Experimental investigations on the mechanical behaviour of SPR joints (Sun and Khaleel, 2007; Sun et al., 2007; Porcaro et al., 2006b) showed that joints using steel rivets can deliver a good crashworthiness and fatigue performance in comparison with spot welded joints, while the riveted joints are less sensitive to corrosion than the welded ones. All of these advantages are a great motivation for a continuous study to push forward the application of SPR joints in the automotive industry.

With the increased use of high strength steel and aluminium sheets in automobile parts in order to reduce the car weight, a lot of researches have been carried out to extend the application domain of the SPR process (Abe et al., 2006, 2008). Abe et al. (2006) have conducted a study on the joinability between mild steel and aluminium alloy sheets; these authors have also succeeded to use the SPR process for joining high strength steel and aluminium sheets with a steel rivet (Abe et al., 2008). Optimum joining conditions have been obtained for a conventional rivet and die used for joining these materials. The optimisation of the riveting process has been conducted both through experimental tests in the laboratory and numerical simulations. The latter has taken a big step forward in recent years, leading to significant improvement in process design as well as cost reduction (Abe et al., 2006, 2008; Porcaro et al., 2006a; Bouchard et al., 2008).

Nowadays, modern car such as the AUDI A2 and the BMW 5 series may contain thousands of steel self-piercing rivets. However, the combination of an aluminium car body and steel rivets makes

* Corresponding author. Address: Structural Impact Laboratory (SIMLab), Centre for Research-based Innovation, Norwegian University of Science and Technology, N-7491 Trondheim, Norway. Tel.: +47 73 59 47 83.
E-mail address: hoang.nguyen-hieu@ntnu.no (N.-H. Hoang).

0020-7683/$ - see front matter © 2009 Elsevier Ltd. All rights reserved.
doi:10.1016/j.ijsolstr.2009.10.009

Nomenclature

L, d	rivet length, rivet diameter
D, h, t	die diameter, die depth, and tip height of the die
σ	effective stress
ε_p	plastic strain
σ_0, Q_i, C_i	Voce parameters defining strain hardening of material
$e_{failure}$	engineering strain at failure
Δx	mechanical interlock of the riveted joint
F_{max}	maximum force characterizing the joint strength
d_{Fmax}	displacement at maximum load F_{max}
F_n	normalised maximum load

recycling a challenge; and aluminium rivets have thus been launched as an alternative. In addition, the exchange of steel rivets with aluminium ones can reduce the vehicle weight, which can contribute to a reduction of fuel consumption and carbon dioxide emission. A quick calculation reveals that the substitution of steel rivets with aluminium ones in the body of an AUDI A2 can save approximately 0.6 kg. Although this gain in weight is not significant compared to the vehicle weight, it still can be very promising in the near future, but probably comes second to the recycling aspect.

Despite all the interesting aspects of the aluminium rivets, no information on this topic has been found in the open literature. All the available literature is focused on the SPR process using steel rivets as well as the mechanical behaviour of the steel SPR joints. The SPR using aluminium rivets is indeed a challenging task, since the strength of aluminium alloys are much weaker than that of steels. The aluminium rivet can be severely deformed when compressed into the plates, and hence no interlock is formed. Thus, a better insight into the joining of aluminium sheets using an aluminium rivet is important in order to have a proper connection. This can only be achieved through an interaction between riveting process tests and corresponding numerical simulations.

In the present paper, an experimental programme has been carried out in order to join two 2 mm-thick sheets in aluminium alloy 6060 in three different tempers (temper W, temper T4, and temper T6) by using an aluminium self-piercing rivets in three different alloys, i.e. 6082-T6, 7108-T5, and 7278-T6. The influence of the die shape on the SPR of aluminium sheets using aluminium rivets was considered by using conventional rivets and dies according to the Boellhoff standards. The test results were exploited in terms of riveting force–displacement curves and cross-sectional geometries of the riveted joints. The experimental results were then compared with the numerical simulations by using a 2D-axisymmetric model. The comparison was carried out to examine the accuracy and the robustness of the 2D riveting model for the analysis of the SPR process using an aluminium rivet. Furthermore, a study of the quasi-static mechanical behaviour of aluminium self-piercing riveted joints under combined loading conditions (i.e. combined pure shear and pure opening forces) was conducted. The influence of the interlock on the mechanical response of the riveted joints was discussed. A comparison between the strength of joint using aluminium and steel rivets was finally done with respect to the force–displacement behaviour.

Table 1
Experimental programme.

Test ID	Top plate	Bottom plate	Rivet	Rivet type	Die
ts1	AA6060-W	AA6060-W	AA6082-T6	C5 × 6	FM 1002018
ts2	AA6060-W	AA6060-W	AA6082-T6	C5 × 6	DZ 0902025
ts3	AA6060-W	AA6060-W	AA7108-T5	C5 × 6	FM 1002018
ts4	AA6060-W	AA6060-W	AA7108-T5	C5 × 6	DZ 0902025
ts5	AA6060-W	AA6060-W	AA7278-T6	C5 × 6	FM 1002018
ts6	AA6060-W	AA6060-W	AA7278-T6	C5 × 6	DZ 0902025
ts7	AA6060-T4	AA6060-T4	AA7108-T5	C5 × 6	FM 1002018
ts8	AA6060-T4	AA6060-T4	AA7278-T6	C5 × 6	FM 1002018
ts9	AA6060-T6	AA6060-T6	AA7278-T6	C5 × 6	FM 1002018

2. Test programme

An extensive test programme was established in order to investigate the SPR of two 2 mm thick aluminium sheets using an aluminium self-piercing rivet, and is presented in Table 1. Plates to be joined were cut from extrusion of aluminium alloy 6060 in two different tempers, i.e. temper T6 and temper T4. However, the temper W was also tested, and was obtained by heat treatment of sheets in T4 temper followed by an immediate quenching in cool water. The rivets were of the Boellhoff type, and were machined using a lathe from the central part of an extruded cylindrical rod made of three aluminium alloys, i.e. 6082 in temper T6, 7108 in temper T5, and 7278 in temper T6. Readers are referred to Sharp (1993) for more details about the plate and rivet tempers. In addition, two conventional dies according to the Boellhoff standards were used in order to study the influence of the die shape. The geometries of the rivet and the die are given in Fig. 2 and Table 2. Nine combinations of the riveted specimens were finally selected in the test programme.

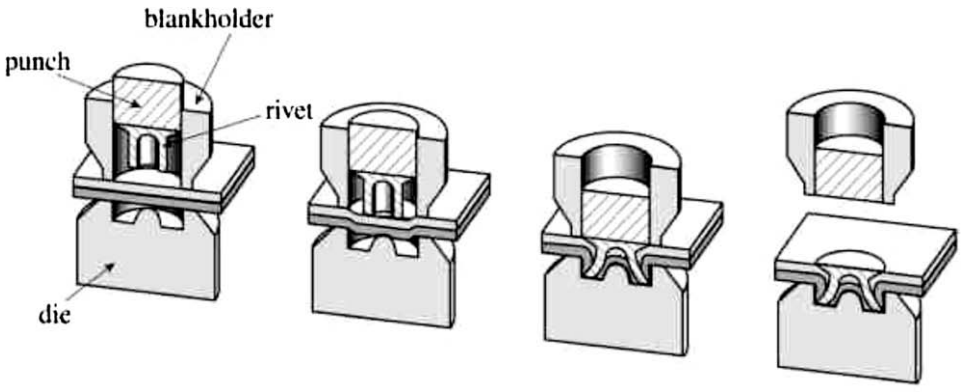

Fig. 1. Self-piercing riveting process (Porcaro et al., 2006a).

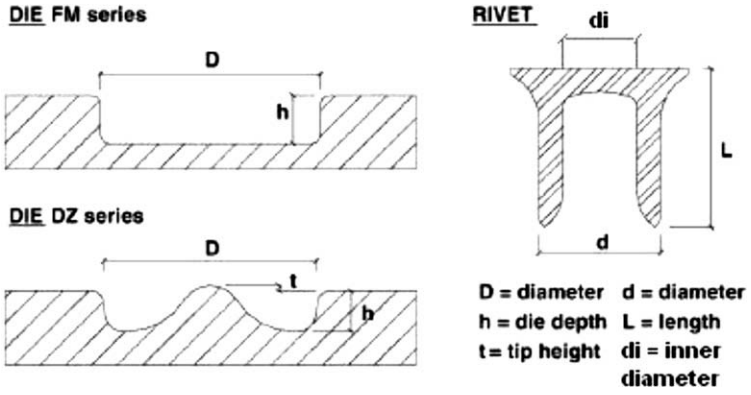

Fig. 2. Geometry definition of the rivet and dies (Porcaro et al., 2006a).

Table 2
Die and rivet geometry.

Parameter	Die FM 1002018	Die DZ 0902025	Rivet C5 × 6
D (mm)	10.000	9.326	–
h (mm)	1.800	1.750	–
t (mm)	–	0.250	–
d (mm)	–	–	5
d_i (mm)	–	–	3.5
L (mm)	–	–	6

3. Material properties

Material data were obtained by means of uniaxial tensile tests. It is to remind that in the present research three commercial aluminium alloys were chosen as rivet material, i.e. AA6082 in T6 temper, AA7108 in T5 temper, and AA7278 in T6 temper, while the aluminium alloy AA6060 in three different tempers (i.e. temper W, temper T4 and temper T6) was used as plate material. Research has shown that these aluminium alloys are quite anisotropic (Lademo et al., 2008; Pedersen et al., 2008). However, in the present paper the alloys are assumed isotropic, i.e. the material properties are assumed independent of the cutting direction of the testing specimens, and the properties of all the alloys were investigated only in the extruded direction. The material tests were performed at room temperature in a hydraulic testing machine under displacement control at a constant strain rate of order $10^{-3}s^{-1}$.

3.1. Rivet material

Three parallel specimens were tested for each rivet material. All specimens are in cylindrical form with a nominal uniform length of 30 mm and diameter of 6 mm, and are machined from the central part of an extruded cylinder which was used for the rivets. The geometry of the specimens is depicted in Fig. 3a. The variation of the diameter in each specimen was less than ±1.2%. All specimens of each rivet material experienced a shear failure as shown in Fig. 4a. Representative engineer stress–strain curves and its corresponding true stress–strain curves up to diffuse necking are plotted in Fig. 4b and c for each rivet material. It is to be noticed from Fig. 4b that the higher strength of the alloy 7278-T6 leads to a reduction in ductility compared with the two other alloys.

The material data were fitted to the Voce isotropic hardening model given by:

$$\sigma = \sigma_0 + \sum_{i=1}^{2} Q_i(1 - \exp(-C_i\varepsilon^p)) \quad (1)$$

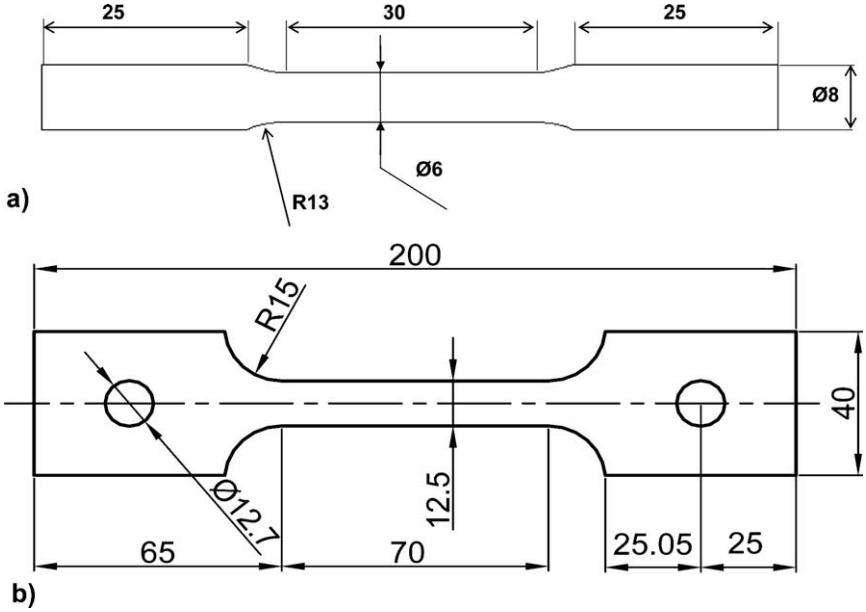

Fig. 3. Specimen geometry for material tests (in mm): (a) rivet material and (b) plate material.

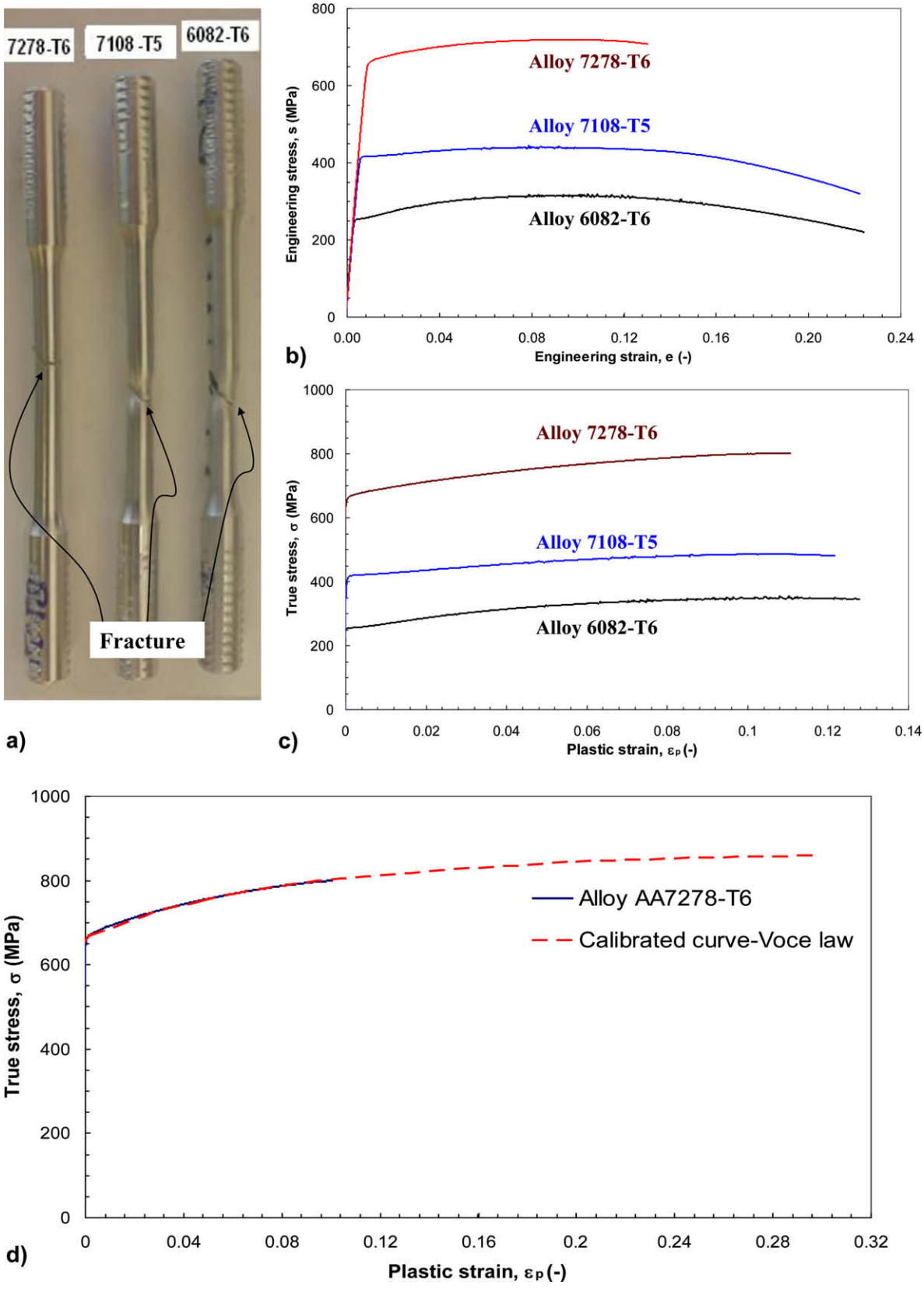

Fig. 4. Quasi-static tensile test results of rivet material: (a) specimens after failure, (b) engineer stress–strain curves, (c) true stress–plastic strain curves, and (d) calibrated stress–strain curve using Voce hardening model.

where ε^p is the plastic strain; σ_0, Q_i and C_i are the material parameters defining the strain hardening. The calculated material constants are found in Table 3, where $e_{failure}$ denotes the engineer strain at rupture. Fig. 4d showed that two exponential terms in

Table 3
Rivet and plate material data.

Material	σ_0 (MPa)	Q_1 (MPa)	Q_2 (MPa)	C_1 (–)	C_2 (–)	$e_{failure}$ (%)
AA7278-T6	651.000	19.849	192.967	633.241	11.342	13.100
AA7108-T5	412.000	89.697	34.673	14.385	1.471	22.300
AA6082-T6	243.000	51.202	64.067	23.053	23.054	22.400
AA6060-T6	170.000	64.773	34.164	13.281	2302.815	–
AA6060-T4	106.000	1.899	141.799	66.618	13.052	17.500
AA6060-W	35.000	76.639	120.597	22.438	1.653	22.230

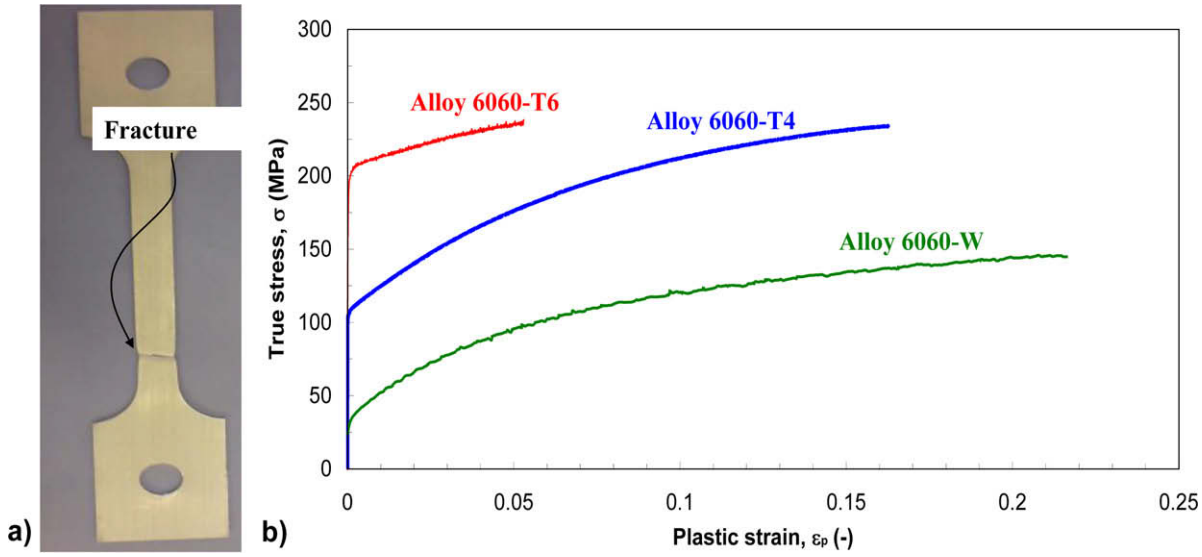

Fig. 5. Tensile test results of plate material: (a) specimen after failure and (b) true stress–strain curves.

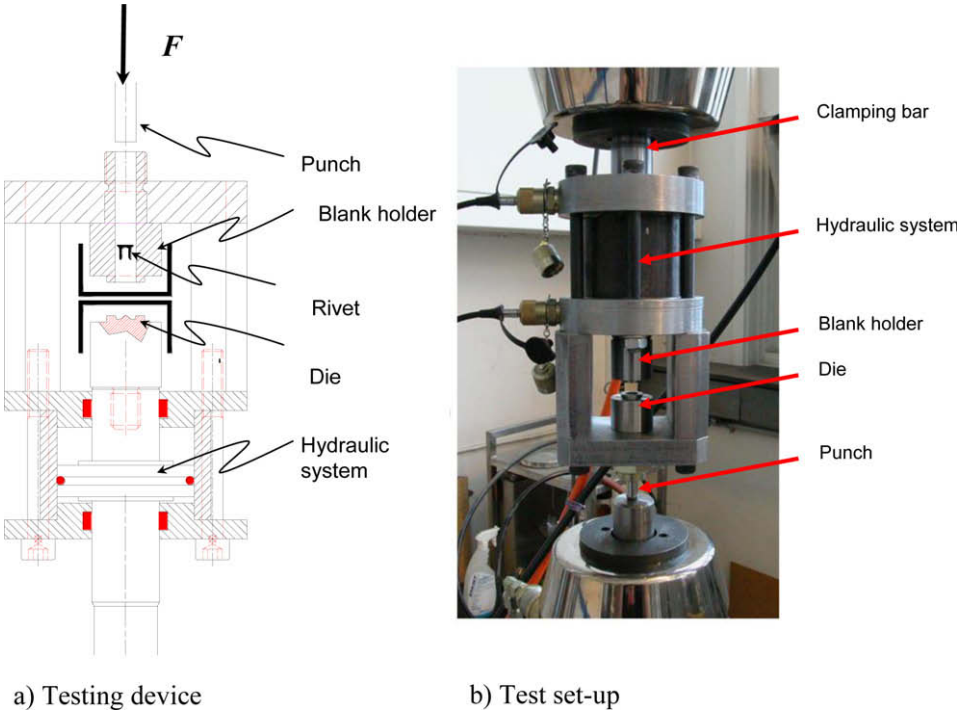

Fig. 6. Testing device for riveting process (Porcaro et al., 2006a).

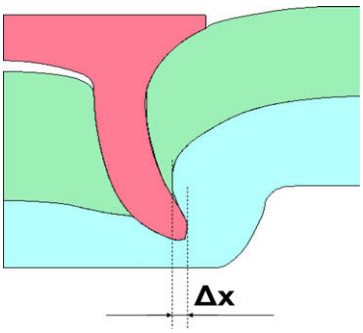

Fig. 7. Definition of the mechanical interlock Δx.

Table 4
Summarization of experimental and numerical values of Δx.

Test ID	Experimental interlock Δx (mm)	Numerical interlock Δx (mm)	Remark
ts1	0.00	0.00	Rivet is compressed
ts2	0.00	0.00	Rivet is compressed
ts3	0.12	0.10	Joining is difficult
ts4	0.00	0.10	Joining is not possible
ts5	0.37	0.28	Joining is possible
ts6	0.30	0.29	Joining is possible
ts7	0.00	0.00	Rivet is compressed
ts8	0.32	0.30	Rivet fracture is observed
ts9	0.29	0.35	Rivet fracture is observed

the multi-component strain hardening model were sufficient for a precise representation of the entire plastic behaviour until the onset of the diffuse necking.

3.2. Plate material

Aluminium alloy AA6060 in three different tempers, i.e. temper W, temper T4, and temper T6 was chosen as plate material in the present study. Temper T6 is a stable temper condition, whereas the properties of the temper T4 and W depend on the aging time of the alloy. Thus, tests were performed to characterize the material behaviour of the aluminium plates in temper W and T4 at the same time the riveting tests were performed. Three tensile plate specimens were used for each temper. The geometry of these specimens with a nominal uniform gauge length of 70 mm and width of 12.5 mm is illustrated in Fig. 3b.

Fig. 5a illustrates a specimen after failure of the plate material. Experimental data were post-processed following the same procedure as for the rivet materials to determine the Voce material constants in Eq. (1), see Table 3. It is to recall that the Voce coefficients of AA6060 in T6 temper were taken from Porcaro et al. (2006a). The true stress–plastic strain curves are presented in Fig. 5b.

4. Self-piercing riveting using aluminium rivets

4.1. Self-piercing riveting process setup

The riveting process was investigated by means of a testing device designed at SIMLab. The device consists of the following parts: (1) punch, (2) blank holder, (3) die, (4) hydraulic system, and (5) clamping bar, see Fig. 6. A detailed description of the device can be found in Porcaro et al. (2006a).

The device is mounted into an Instron testing machine by fixing the clamping bar into the machine. The die is pushed toward the blank holder to clamp the specimen which is positioned between the die and the blank holder during the riveting process. The clamping pressure is maintained constant during the process. The punch pushes the rivet through the hole in the blank holder.

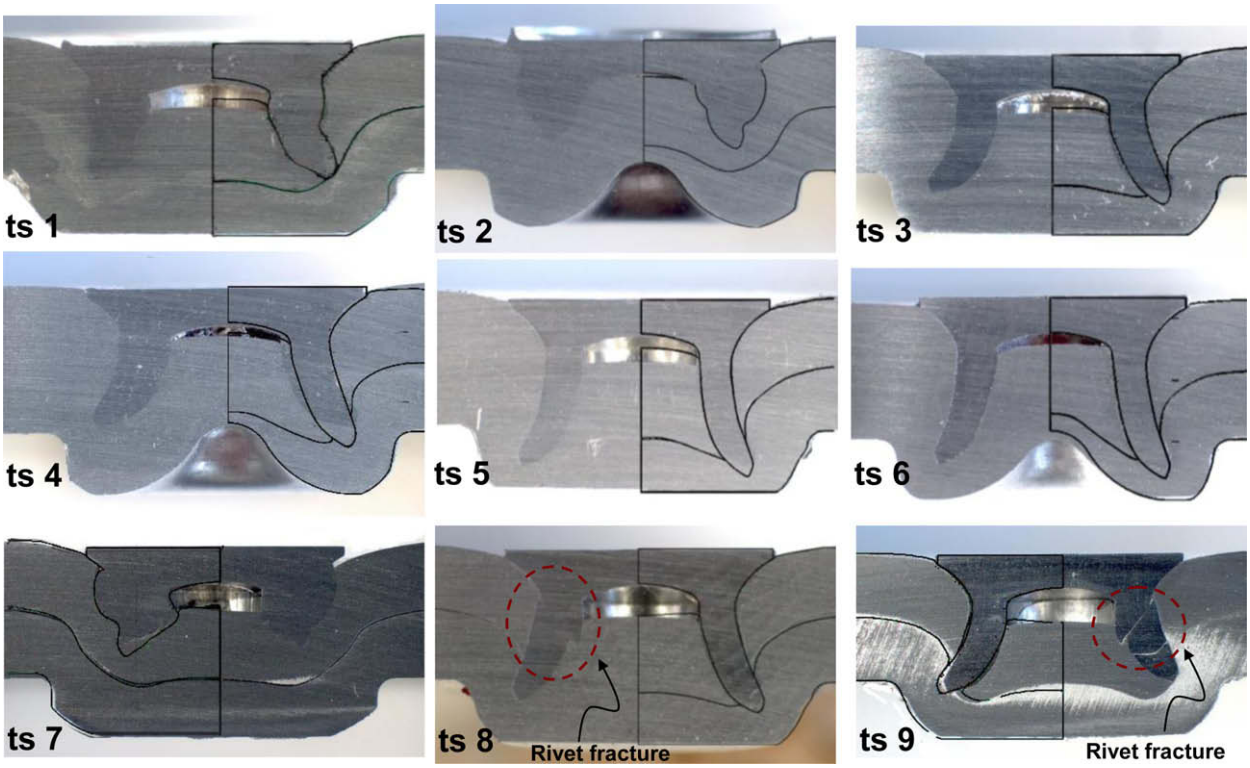

Fig. 8. Experimental and numerical cross-sectional geometries for all the specimens (black lines represent the numerical cross-sectional shapes).

The tests were conducted under displacement control at quasi-static strain rate. The clamping pressure between the blank holder and the die is released at the end of the tests, and the specimen is removed from the test device. Force–displacement histories were recorded during the tests.

4.2. Riveting test results and discussions

Twenty-seven tests were performed in order to investigate the riveting force–displacement response, corresponding to nine combinations in the initial test matrix (Table 1), i.e. three repetitions for each combination. The cross-sectional shapes of riveted joints were also investigated. The interlock parameter Δx, which is defined in Fig. 7, was used to specify the quality of the SPR connections. The measurement of the experimental interlock was done from a picture of the cross-section with a reference scale. The accuracy of the measurement was estimated to ±0.01 mm. The experimental values of Δx for all specimens are summarised in Table 4. A too small value of Δx may lead to a bad mechanical strength of the riveted joint.

Table 4 and Fig. 8 show that the piercing of aluminium sheets in alloy 6060-T6 is possible when the rivet is in alloy 7278-T6. The rivet went through the upper and flared into the bottom plate and formed an interlock. However, fracture in the rivet was observed, see Fig. 8, test ts9. The rivet failure was also obtained when using a rivet in alloy 7278-T6 to join two plates in alloy 6060-T4, see Fig. 8, test ts8. The rivet fracture is believed to be due to the reduced ductility for high strength aluminium alloys, see Table 3. It is of interest to notice that the observed rivet failure is not axisymmetric. Reducing the strength of the rivet can avoid fracture in the rivet; however, the rivet strength close to that of the plates might lead to a severe deformation of the rivet and no formation of an interlock, see Fig. 8, test ts7.

Heat treatment of the 6060-T4 plates to be joined into W temper was then employed to facilitate the riveting process, and to decrease the risk of the fracture in the rivet. Although the softening of the aluminium plates eased the driving of the aluminium rivet through the upper plate, an acceptable interlock was not obtained with the rivet in 6082-T6, see Table 4 and Fig. 8, tests ts1 and ts2. A significant deformation of the rivets in 6082-T6 was observed for both dies. Even when the driving of the rivet through the upper plate was obtained with the rivet in 7108-T5, the mechanical interlock Δx formed within the bottom plate was too small to provide a joint with good mechanical behaviour, see Table 4 and Fig. 8, tests ts3 and ts4. A proper connection was solely obtained when using a high-strength rivet in alloy 7278-T6 as shown in Fig. 8, tests ts5 and ts6. Moreover, a visual comparison between the cross-sectional geometries of the two specimens ts1 and ts2 (see Fig. 8) showed that using a FM die can facilitate the riveting process better than using a DZ die. Thus, in addition to the adjustment of the strength of the rivet material to that of the plate material, the die geometry can also be optimised to deliver a better SPR connection.

Typical riveting force–displacement curves recorded during the riveting process are presented in Fig. 9. It is to be noticed from Fig. 9a that the first part of the force–displacement curve starts with a small slope followed by a higher one; the latter indeed characterizes the penetration of the rivet into the upper plate. The small slope at the beginning of the curve is believed to be due to some elastic deformation of the testing device, and is thus not related to the riveting process. The initial slope was then removed; the force–displacement curves were shifted back to the origin as shown in Fig. 9b. The experimental force–displacement curves for all the specimens after the shifting are illustrated in Fig. 10. It is to note that a small scatter in the measured riveting force was observed for most of the tests.

5. Numerical simulations of the riveting process

The main objective of this section is to examine whether the 2D-axisymmetric model, which was originally proposed by SIMLab for modelling the SPR process using a steel rivet, is still appropriate for aluminium rivets. The model has already been described by Porcaro et al. (2006a). However, the main details of the model are recalled in Section 5.1 for the sake of completeness. The validation of the 2D model is discussed in Section 5.2 through a comparison between numerical and experimental results in terms of the load–displacement curves and cross-sectional geometries.

5.1. Numerical model of the SPR process

The 2D-axisymmetric model was generated in the commercial finite element code LS-DYNA, using four-node 2D-axisymmetric elements with four Gauss points, and stiffened-based hourglass control (assumed strain co-rotational stiffness form). The model contained six different parts: (1) rivet, (2) bottom plate, (3) top plate, (4) punch, (5) blank holder, and (6) die, see Fig. 11. The punch, blank holder and die were assumed to be rigid, while the material of the rivet and sheets which undergo plastic deformation during the riveting process were modelled as elastic–plastic materials, adopting an isotropic strain-hardening rule, and the associated flow rule in the plastic domain (*MAT_MODIFIED_JOHNSON_COOK). Contact was modelled using an automatic 2D single-surface penalty formulation available in LS-DYNA. A Coulomb friction model was used at the interface between each part. The static coefficient of friction at the interface between the rivet and the plates, and between the two plates was set to 0.15. The corresponding friction coefficient between the plates and other tools was set 0.30. The sheets were clamped between the die and the bank holder with a constant and significantly high force of 1000 N. A displacement was then prescribed to the punch in order to push the rivet through the sheets until the joint was formed.

A fine mesh size of 0.1 mm × 0.1 mm was used in both the rivet and plates in combination with the *r*-adaptivity remeshing method in order to deal with the element distortion problem that can be

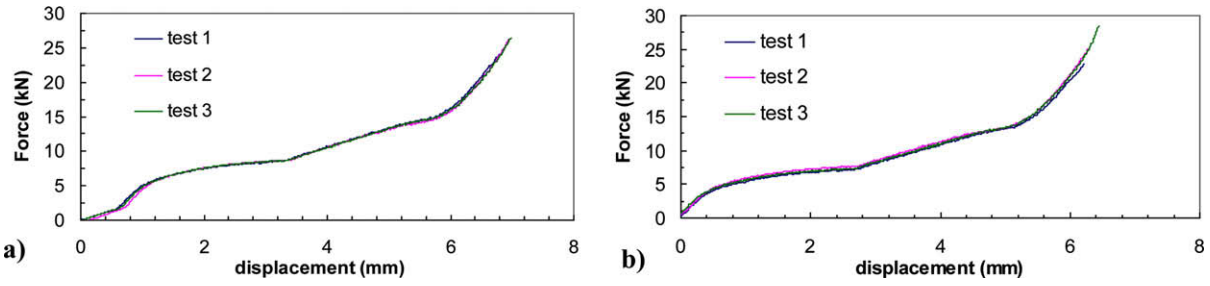

Fig. 9. Typical riveting force–displacement curves: (a) before shifting and (b) after shifting.

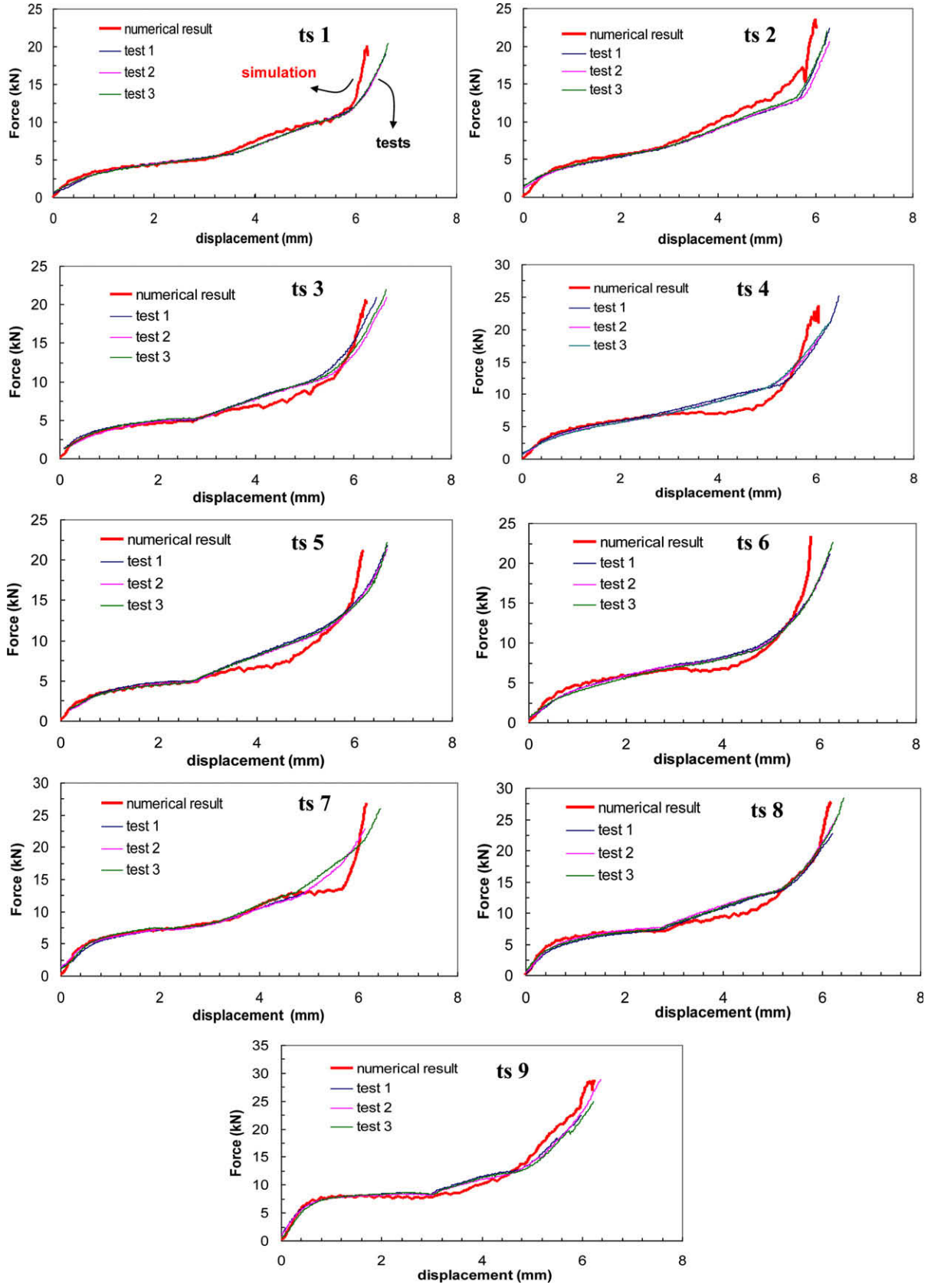

Fig. 10. Experimental and numerical force–displacement curves for all the specimens.

induced when the rivet and plates undergo a very high plastic deformation. A failure criterion based on part thickness considerations was also used in order to allow the separation of the upper sheet in two parts when a user-defined thickness (i.e. 0.2 mm) of

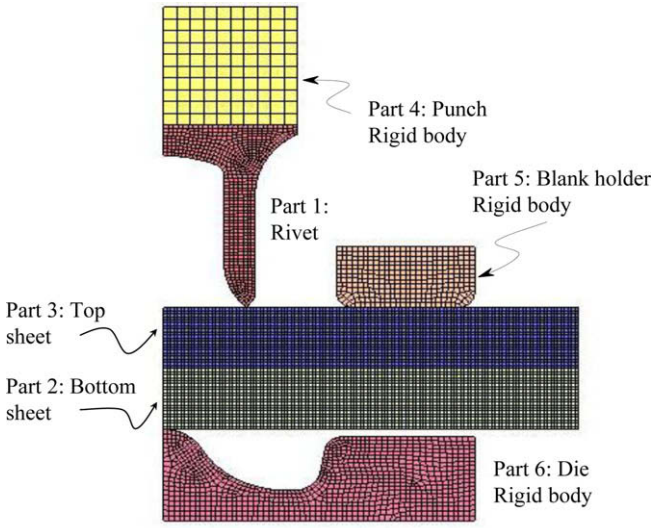

Fig. 11. Numerical model and initial mesh.

the sheet is reached. This "kill element" methodology does not cause a significant volume loss since the number of elements deleted is small, and the element deletion procedure can be activated only once during the simulation. Fig. 12a and b, respectively, shows a view in the critical area of plastic strain before and after the complete separation is achieved.

Simulations were run by means of an explicit solver which can lead to important computational time. However, the calculation time can be reduced by increasing the punch velocity compared to the physical riveting. The virtual velocity was chosen so that the deformation of the rivet and plates was not affected, and the dynamic energy involved in the riveting process remained small compared to the rate of the internal energy. Fig. 13 shows a comparison of the rivet deformation of two simulations at two different velocities. Here, the punch velocity in the first simulation (Fig. 13a) was 100 times greater than that in the second simulation (Fig. 13b); the deformations of two rivets were indeed similar.

5.2. Numerical analysis and discussions

The experimental database was used to validate the 2D-axisymmetric model. The cross-sections of all the specimens were first

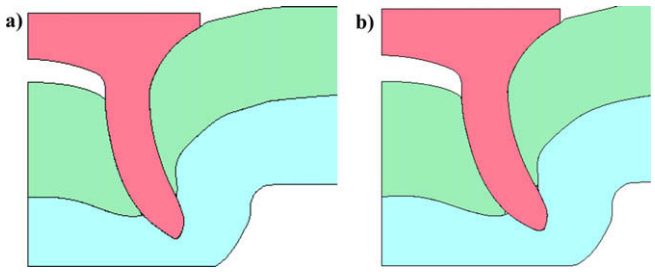

Fig. 13. Numerical rivet deformation: (a) explicit result with increased velocity and (b) explicit result with normal velocity.

compared to the numerical results. Fig. 14 shows how the final configuration of the numerical result can be compared to experiments; the border of the numerical geometry was extracted and superposed to the experimental cross-section. The comparison for each combination was then presented in Fig. 8 and Table 4. Good agreement between simulations and experiments has been found for most of the specimens. It is to notice that the present model was not able to capture the rivet failure observed for the coupons ts7, ts8, and ts9 as no failure criterion of the rivet was taken into consideration in the numerical simulations. However, the present numerical model seems to capture the overall deformation mode of the rivet and plates quite well.

The evolution of the punch force versus displacement during the riveting process was also analysed; a representative comparison between the numerical and experimental force–displacement curves of the riveting process is presented in Fig. 15. As can be observed in Fig. 15a and b, the force–displacement curves can generally be divided in four parts characterizing four different stages during the riveting process: Part 1 – bending: the rivet starts to penetrate the upper plate, but the main deformation mode is the bending of the plate; Part 2 – shearing: the rivet is driven through, and shears off the upper plate, Part 3 – spreading: the rivet goes through the top sheet and flares into the bottom one, Part 4 – setting: the rivet enters the lower sheet, causing a filling of the die to create an mechanical interlock in the final step. A slight difference between experiments and simulations was observed for Part 3; the numerical force slightly descended at the beginning of Part 3 before climbing up to reach the same level as the experimental force at the end of Part 3. The force declination at the beginning of Part 3 may mainly result in the decrease of the stiffness when the element deletion algorithm is triggered (at the moment when

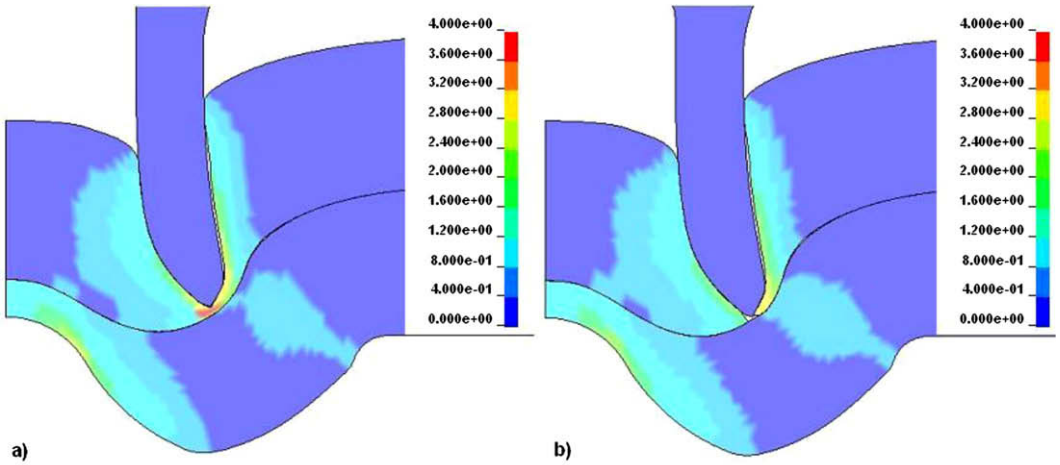

Fig. 12. Zoom view of the plastic strain state: (a) before the fracture of upper sheet and (b) after the fracture.

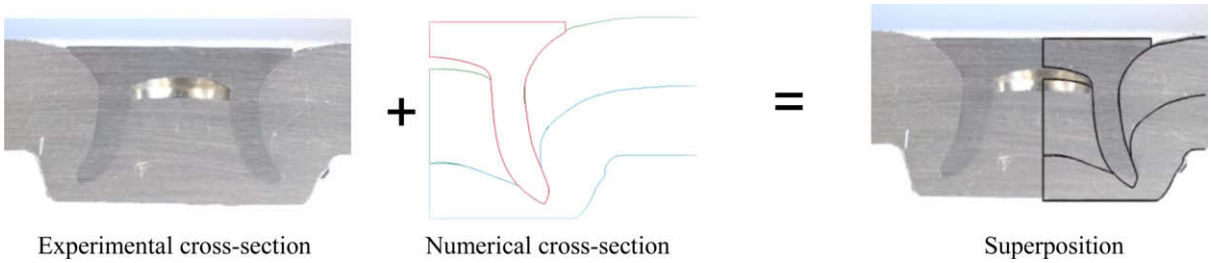

Fig. 14. Comparison between experimental and numerical cross-section.

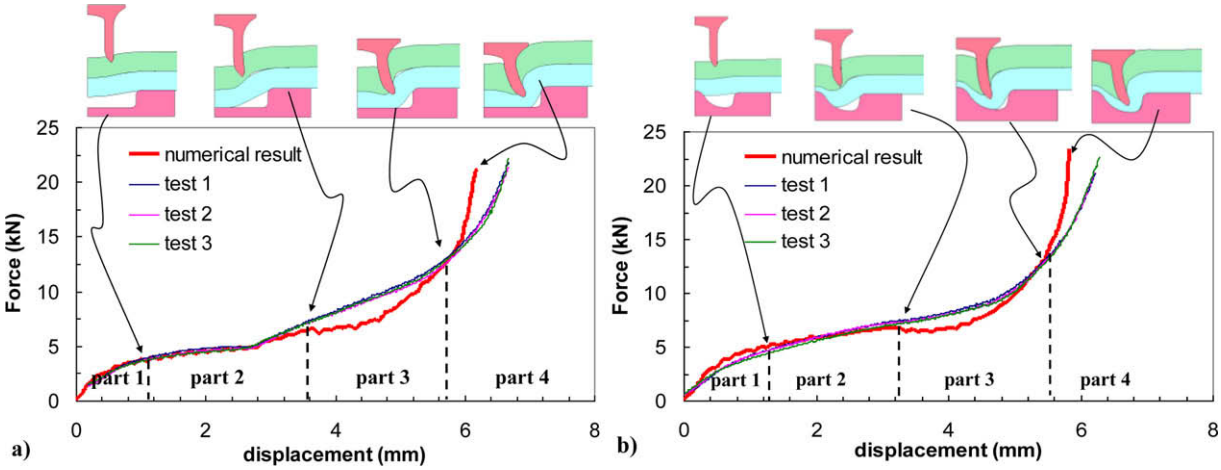

Fig. 15. Comparison of the force–displacement curve between tests and simulation: (a) with a FM die and (b) with a DZ die.

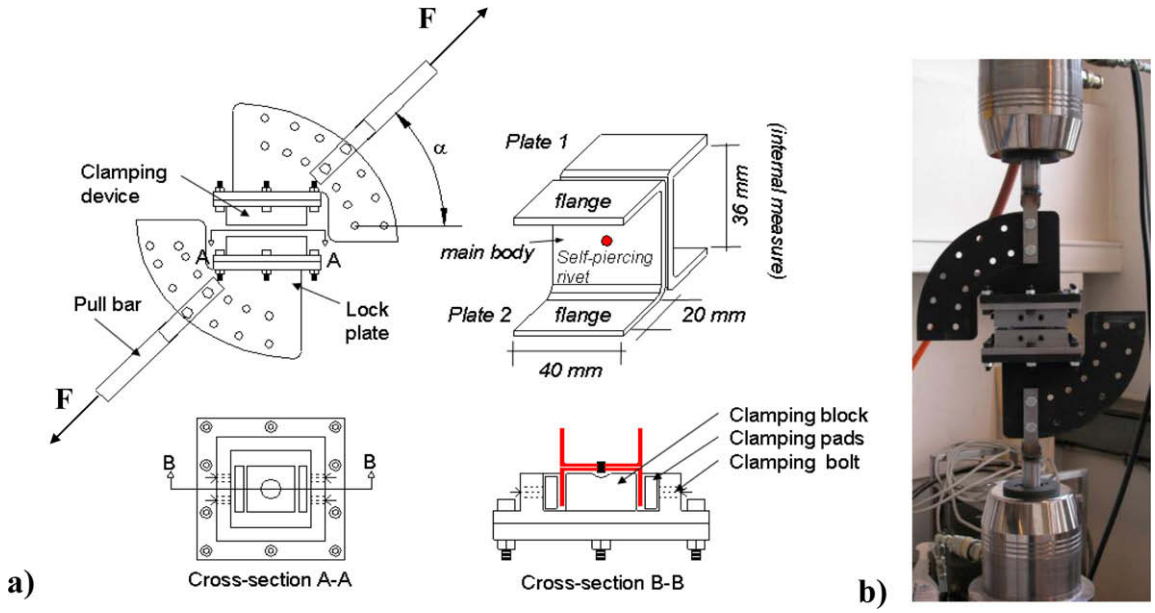

Fig. 16. (a) Geometry of the test fixture and U-shaped specimens. (b) Test set-up for pure pull-out test (Porcaro et al., 2004).

the rivet perforates the upper plate). Moreover, the two curves in Fig. 15a and b are different; and it is caused by a different shape of dies. It can be seen from Fig. 15a that when using a FM die an abrupt transition of the force–displacement curve in Part 2 was remarkably observed when the bottom plate went into contact with the FM die. This phenomenon was not observed when using a DZ die, see Fig. 15b, since the plates to be joined were always in contact with the DZ die; the recorded force was gradually increasing with the increase of the punch displacement. The difference between experiments and simulations were also observed at the end of the riveting process (Part 4). This difference may be a result of some elastic deformation of the experimental devices under the very high force required for the joining process (approximately 25 kN).

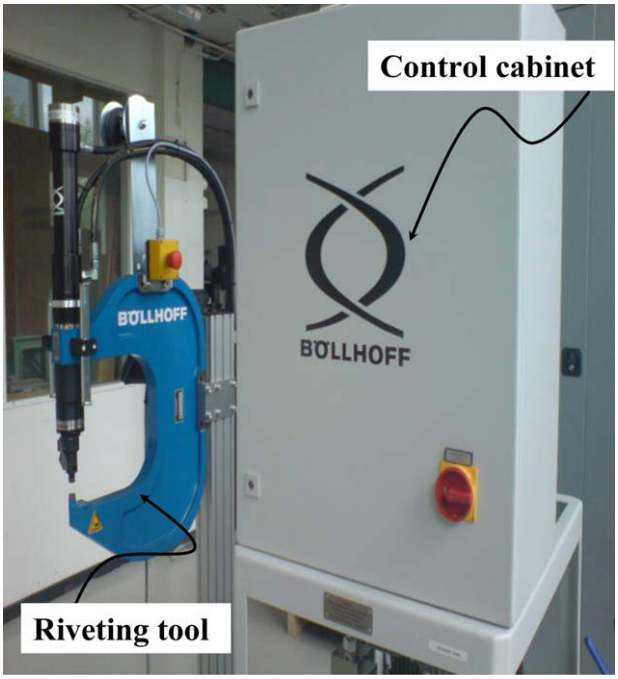

Fig. 17. Boellhoff riveting machine.

Table 5
Material parameters of alloy 6060.

Material	Yield stress, σ_0 (MPa)	Ultimate engineering stress, S_u (MPa)
Alloy 6060-T4 (Porcaro et al., 2006b)	73	158
Alloy 6060-W after 3 days	53	154

Comparisons between experiments and simulations in terms of force–displacement curves for all the combinations are found in Fig. 10. Elastic deformations of the testing device are removed from all recorded force–displacement curves; and good comparisons were then obtained for most of the specimens. The decrease of the numerical force at the beginning of the third stage compared with experiments (Part 3) was observed in some cases as stated previously. This was assumed to be due to the element erosion algorithm triggered when the upper plate was cut off at the beginning of this part. When the top plates were not cut off as for the specimens ts1, ts2 and ts7, numerical and experimental results in Part 3 were in a good agreement, see Fig. 10.

6. Mechanical behaviour of aluminium SPR joints

6.1. Mechanical test setup

The mechanical behaviour of an aluminium SPR joint was studied by using a specimen geometry which is composed of two identically U-shaped elements joined together in the central part with one aluminium rivet. The mechanical tests were conducted under different loading conditions using a test fixture presented by Porcaro et al. (2004). The testing device is comprised of two identical test units, see Fig. 16. Each unit has a clamping system which consists of actuator bolts and clamping pads for gripping one U-shaped element of the testing coupon. The fixture was designed so that shear and tensile loads can be combined. The tensile/shear load ratio is characterized by the angular position α between the centreline of coupons and the loading direction. The latter is in turn defined by two pull bars positioned in a straight line that crosses the rivet centre. The pull bar system can be considered as a rigid body. Three loading directions were considered in the present study, i.e. $\alpha = 0°$, $\alpha = 45°$, $\alpha = 90°$, corresponding to pure shear, combined loading conditions, and pure pull-out, respectively.

After mounting the pull bars into the Instron machine, mechanical tests were then conducted under displacement control with a rate of displacement of approximately 2 mm/min. The load–displacement histories were simultaneously recorded during the test-

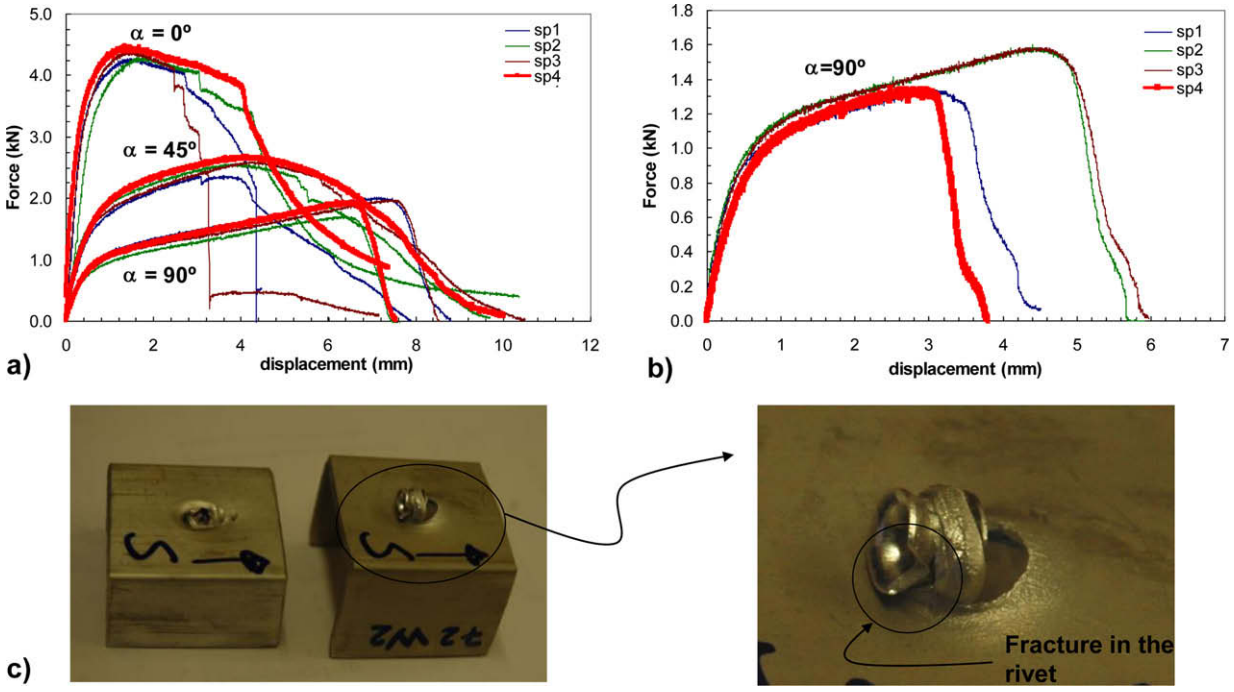

Fig. 18. (a) Experimental force–displacement curve for U-shaped specimens ts5 under different loading directions; (b) scatter in result for specimens ts3; and (c) fracture in the rivet in pure shear tests.

Table 6
Experimental mechanical test results.

Loading condition	Specimen ID	Rivet AA7108-T5 (ts3)		Rivet AA7278-T6 (ts5)	
		F_{max} (kN)	d_{Fmax} (mm)	F_{max} (kN)	d_{Fmax} (mm)
Pure shear loading, $\alpha = 0°$	sp1	4.065	1.263	4.280	1.466
	sp2	4.123	1.238	4.310	1.850
	sp3	4.100	1.054	4.398	1.491
	sp4	3.979	1.110	4.467	1.482
Combined loading, $\alpha = 45°$	sp1	2.045	2.066	2.350	3.710
	sp2	2.300	2.910	2.570	3.920
	sp3	1.970	2.157	2.600	4.383
	sp4	1.711	1.740	2.670	4.164
Pure pull-out loading, $\alpha = 90°$	sp1	1.340	3.100	2.020	7.150
	sp2	1.600	4.400	1.720	6.360
	sp3	1.590	4.500	1.966	7.580
	sp4	1.340	2.890	1.927	6.570

ing, and the recorded displacement is representative of the deformation of the test specimen. The tests were terminated when the two components of the specimen were completely separated.

As shown in Table 4, only two combinations ts5 and ts6 could provide a proper connection with a significantly important interlock. Within this framework, the mechanical behaviour of combination ts5 was studied. In addition, the combination ts3 was also subjected to mechanical tests in order to investigate the influence of the interlock on the mechanical behaviour. Three test specimens for each combination were assembled by means of a Boellhoff SPR machine, see Fig. 17. This is a standard machine which is generally used for an automated assembly process in the automotive industry. Compared to the SIMLab device, the Boellhoff system allows for a shorter time of assembly (approximately 0.2 s). Furthermore, the Boellhoff riveting system is both hydraulic pressure- and displacement-controlled. The thickness of the plates to be joined is first checked between the die and the blank holder during a preclamping step for safety control; once the latter is done the riveting process is then triggered. When the pre-set pressure and the specified distance of rivet penetration are reached, the return stroke of the blank holder is activated to terminate the riveting process. In order to study the influence of the riveting process on the mechanical behaviour of the riveted joints, one additional specimen was joined by using the SIMLab device described in Section 4.1, and then subjected to mechanical tests.

Prior to mechanical testing, all specimens under investigation were exposed to room temperature for approximately 3 days in order to get a stable condition of the materials to be joined (i.e. by natural aging). Material properties of the plates after a natural aging phase of 3 days were obtained from uniaxial tensile tests, and are given in Table 5.

6.2. Mechanical test results and discussions

Typical force–displacement curves of the combination ts5 under three different loading angles are showed in Fig. 18a where sp1, sp2 and sp3 denote the three first specimens that were riveted by means of the Boellhoff system, and sp4 denotes the one which was joined by using the SIMLab device. The recorded force–displacement curves were then post-processed to get maximum load, F_{max}, and displacement at maximum load, d_{Fmax}, as function of loading angle α and rivet combination. The results are showed in Table 6.

It can be noticed that the mechanical behaviour of an aluminium SPR joint under combined loading follows the general trend that was observed for corresponding steel riveted joints, i.e. the maximum load as well as the initial stiffness increases, whereas the displacement at maximum load decrease with the decrease of the loading angle α. Scatter in the measured data are evident; especially for the combination ts3 as shown in Fig. 18b. The scatter is believed to be mainly due to the quality of the joint, since for the combination ts3 the mechanical interlock Δx, which was defined in Fig. 7, was not sufficient to provide a stable mechanical response. When the interlock is increased as observed for the combination ts5, a small variation in the mechanical results has been found, see Fig. 18a. Moreover, it is to notice from Fig. 18a that the riveting process seems to have no influence on the static behaviour of riveted joints. The obtained result from the specimen sp4 using the SIMLab device was similar to that of the other specimens. The small difference in result observed after the maximum force is reached is obviously due to the fracture of the rivets as shown in Fig. 18c.

Fig. 19 shows a representative comparison between the mechanical responses in different loading directions using aluminium and steel self-piercing rivets. The latter was taken from Porcaro et al. (2006b); two 2 mm thick plates in aluminium alloy 6060-T4 were joined using a rivet made of boron steel with the same geometry as used for the aluminium rivets and a DZ die. It is interesting to notice from Fig. 19a that the rivet material did not affect the initial stiffness of the mechanical force–displacement curves, but only the maximum force as well as the displacement at maximum load. Here, when the interlock is too small as for the combination ts3, a significant reduction in F_{max} as well as in d_{Fmax} was observed as shown in Fig. 19a. When a significant interlock was obtained as for the combination ts5, the riveted connections using an aluminium self-piercing rivet can deliver a good static performance in comparison with a steel rivet. However, it is to recall that the plate materials used in the present study were not in T4 temper as used by Porcaro et al. (2006b), but indeed in W temper followed by 3 days of natural aging, see Table 5. In order to study the influence of solely the strength of the rivet material on

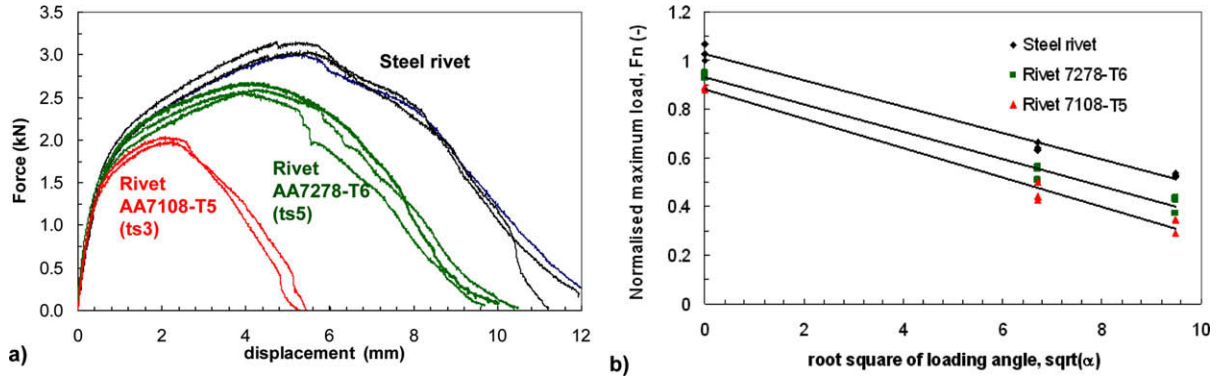

Fig. 19. Comparison of single-joint strength between aluminium rivet and steel rivet: (a) combined loading with $\alpha = 45°$, (b) normalised maximum load versus loading angle curves.

the riveted joint's strength, the normalised maximum load, F_n, is defined, and is plotted versus the root square of the loading angle $\sqrt{\alpha}$ in Fig. 19b. The normalised maximum load is given by:

$$F_n = \frac{F_{max} \times 1000}{s_u \times L \times D} \quad (2)$$

where L and D are parameters of the rivet geometry, and s_u is the ultimate engineering stress of the plate material, and F_{max} are the maximum load. It can be seen from Fig. 19b that the normalised force F_n is indeed a linear function of the root square of the loading angle $\sqrt{\alpha}$. Moreover, the variation of the strength of aluminium riveted joints as a function of the loading angle follows the same trend as for the steel riveted joints. Here, it is interesting to see that the difference in F_n between the steel rivets and rivets in alloy 7278-T6 is of order of 10%; and this difference is believed to be mainly due to the rivet material. This means that the strength of the rivet material may also have an influence on the behaviour of the riveted joints in addition to the other riveting parameters, e.g. the plate material, the plate thickness, etc.

7. Conclusions

The possibility of replacing a steel self-piercing rivet with an aluminium rivet, when using a conventional die in accordance with the Boellhoff standards was investigated in the present work. An experimental programme was defined and reported on the riveting process using an aluminium self-piercing rivet and two conventional dies of the Boellhoff type to join two 2 mm thick aluminium plates in alloy 6060 in three different tempers (temper W, temper T4, and temper T6). Three commercial alloys were used as rivet material, i.e. AA6082-T6, AA7108-T5 and AA7278-T6. The riveting test results were studied in terms of riveting force–displacement curves and cross-sectional geometries of the riveted joints. The tests have been shown that a proper joint can be obtained when using a rivet in alloy 7278-T6 to join two plates in alloy 6060-W. Here, the heat treatment of the 6060-T4 plates into W temper was needed in order to avoid fracture in the rivet as observed when riveting two plates in alloy 6060 tempers T4 and T6. The experimental results also revealed that in addition to the adjustment of the rivet strength to the plate strength, an optimised die shape might lead to a riveted joint with a better quality.

The riveting test results were also used as a database to validate a 2D-axisymmetric model generated in the explicit commercial LS-DYNA finite element code. Simulations were performed using an explicit solution technique. An *r*-adaptive method together with a mesh size of 0.1 mm × 0.1 mm was used to deal with the element distortion problem encountered during the riveting process. The simulation results were in good agreement with the experiments, both with respect to the force–displacement curves as well as the cross-sectional shapes of the rivet and plates. However, the present model was not able to capture the fracture in the rivet exhibited in some combinations.

The mechanical behaviour of aluminium SPR joints under quasi-static load was also studied and compared with that of the corresponding steel ones. It showed that the rivet material did not influence the initial stiffness of the mechanical response, but only the maximum force and the displacement at maximum force. The mechanical interlock had a significant influence on the mechanical behaviour of the riveted connections. It demonstrated that a small interlock led to an important degradation of the mechanical behaviour. However, it transpires that aluminium SPR joints can provide a good static strength in comparison with the steel ones. A difference in strength of approximately 10% was reported. It has also been showed that the normalised maximum force F_n was a linear function with respect to the square root of the loading angle.

Acknowledgements

Thankful acknowledgement is specially made to the Structural Impact Laboratory (SIMLab), Centre for Research-based Innovation (CRI) at the Norwegian University of Science and Technology (NTNU), for their financial support.

References

Abe, Y., Kato, T., Mori, K., 2006. Joinability of aluminium alloy and mild steel sheets by self-piercing rivet. Journal of Materials Processing Technology 177, 417–421.

Abe, Y., Kato, T., Mori, K., 2008. Self-piercing riveting of high tensile strength steel and aluminium alloy sheets using conventional rivet and die. Journal of Materials Processing Technology, doi:10.1016/j.jmatprotec.2008.09.007.

Bouchard, P.O., Laurent, T., Tollier, L., 2008. Numerical modelling of self-pierce riveting – from riveting process modeling down to structural analysis. Journal of Materials Processing Technology 202, 290–300.

Lademo, O.-G., Pedersen, K.O., Berstad, T., Furu, T., Hopperstad, O.S., 2008. An experimental and numerical study on the formability of textured AlZnMg alloys. European Journal of Mechanics – A/Solids 27, 116–140.

Pedersen, K.O., Lademo, O.-G., Berstad, T., Furu, T., Hopperstad, O.S., 2008. Influence of texture and grain structure on strain localisation and formability for AlMgSi alloys. Journal of Materials Processing Technology 200, 77–93.

Porcaro, R., Hanssen, A.G., Aalberg, A., Langseth, M., 2004. Joining of aluminium using self-piercing riveting: testing, modelling and analysis. International Journal of Crashworthiness 9, 141–154.

Porcaro, R., Hanssen, A.G., Langseth, M., Aalberg, A., 2006a. Self-piercing riveting process: an experimental and numerical investigation. Journal of Materials Processing Technology 171, 10–20.

Porcaro, R., Hanssen, A.G., Langseth, M., Aalberg, A., 2006b. The behaviour of a self-piercing riveted connection under quasi-static loading condition. International Journal of Solids and Structures 43, 5110–5131.

Sharp, M.L., 1993. The metal aluminium. In: Sharp, M.L. (Ed.), Behavior and Design of Aluminum Structures. McGraw-Hill, New York, pp. 1–16.

Sun, X., Khaleel, M.A., 2007. Dynamic strength evaluations for self-piercing rivets and resistance spot welds joining similar and dissimilar metals. International Journal of Impact Engineering 34, 1668–1682.

Sun, X., Stephens, E.V., Khaleel, M.A., 2007. Fatigue behaviours of self-piercing rivets joining similar and dissimilar sheet metals. International Journal of Fatigue 29, 370–386.